ADVANCED MATERIALS
www.advmat.de

External-Strain Induced Insulating Phase Transition in VO_2 Nanobeam and Its Application as Flexible Strain Sensor

By *Bin Hu, Yong Ding, Wen Chen,* Dhaval Kulkarni, Yue Shen, Vladimir V. Tsukruk,* and *Zhong Lin Wang**

Vanadium dioxide (VO_2), one of the most extensively studied structures in the correlated electron material family, undergoes a first-order insulator (low-temperature) to metal (high-temperature) transition (MIT) near room temperature (~68 °C), which is simultaneously accompanied by a structural transition from a monoclinic (M) insulating structure to a rutile (R) metallic phase. Comparison of the percolative nature of MIT in two-dimensional polycrystalline VO_2 thin films or VO_2 nanoplatelets,[1,2] and one-dimensional VO_2 morphology, especially on the nanometer-scale, is finding its way into functional device applications owing to its single-crystal structure with homogeneous phase and dislocation-free volume along with homogeneous domains. These structural characteristics account for the occurrence of MIT over a much narrower temperature range.[3,4] Furthermore, a one-dimensional structure can be a good candidate to load the tunable external strain for electrical and optical properties control. Recently, Cao et al. provided a novel way to control the periodic insulating and metallic phase domains along the VO_2 nanobeams by continuously tuning the strain, and the MIT temperature can be lowered to room temperature, which is beneficial for functional VO_2 device and sensor applications.[4,5]

To date, most of the works have been focused on studying the physics behind MIT[6,7] for device fabrication owing to the sharp change in conductivity by several orders of magnitude when heated.[8–10] However, VO_2 can undergo an insulating crystallographic structure transition at room-temperature by applying uniaxial high pressure along the [110] direction of the rutile phase ($R_{[110]}$) in pure VO_2 or doping high Cr in the initial insulating phase (M_1 insulator) turning it into another stabilized insulator phase (M_2 insulator), which is known as a monoclinic M_1–M_2 transition.[11,12] In contrast to the abrupt change from a bright reflection M phase to a dark reflection R phase over MIT temperature, the M_1–M_2 transition is difficult to monitor under optical microscopy. Recently, the presence of an M_2 phase in the R phase when heating the clamped single crystal VO_2 nanobeam has been observed by X-ray diffraction, and the co-existence of R, M_1, and M_2 phases in the surface clamped nanobeam under heating is a result of minimizing the system energy when subjected to external strain.[13] Raman scattering has been known to be an excellent non-destructive tool to study the physical transition, chemical composition, and lattice dynamics of various organic and inorganic nanomaterials.[14–18] It has been used to probe the diameter, chirality, orientation, stress, and deformation in carbon nanotubes and other inorganic nanostructures such as GaN nanowires and anisotropic ZnO nanostructures,[19–22] and recently, it was used to observe the phase transition in a single heated VO_2 nanobeam and correlate it with the electrical characteristics of the nanobeam. The M and R phases in the VO_2 nanobeam have been demonstrated to be highly sensitive to internal stress in the crystalline structure. The appearance and shifts in the peak positions of M_1 and M_2 phases have been employed to monitor and correlate the phase transition with the applied strain.[23,24] MIT has already been exploited to fabricate ultra-sensitive transition-edge sensors and fast optical shutters.[8,9,25] The transition between the M_1 and M_2 insulator can be utilized in developing fast and reproducible strain sensors or logic switches. In this study, we probe the room temperature M_1–M_2 phase evolution in a single end-clamped VO_2 nanobeam subjected to tensile and compressive stresses along the long axis using confocal Raman microscopy. Furthermore, electrical characteristics support it with the corresponding phase transitions monitored from the Raman measurements. These measurements aided as a working principle the fabrication of a phase-transition-based strain sensor. The device showed an excellent control over the phase transition and the electrical resistance resulting in a high gauge factor, quick response time and good reproducibility at room temperature, making it ideal for measuring strain in nanometer-scaled devices.

Nanobeams with lengths ranging from tens to more than a hundred micrometers were obtained at the edge of the substrate, and most of them were sticking out of the substrate like natural cantilevers, as shown in **Figure 1a**, making them lift down easier for device fabrication.[26] Compared to bulk or film, the low dimensional and the single-crystal nature of the nanobeams can withstand a much higher uniaxial strain without plastic deformation or fracture.[4,27] On subjecting the nanobeam to high lateral forces, it buckles to form an 'Ω'-shaped structure (insert in Figure 1a), thereby demonstrating the flexible and robust nature of the VO_2 nanobeam. A detailed morphology study shown in Figure 1b further revealed that the nanobeam exhibits a clear rectangular-like cross section with

[*] Dr. B. Hu, Y. Ding, D. Kulkarni, Y. Shen, Prof. V. V. Tsukruk, Prof. Z. L. Wang
School of Materials Science and Engineering
Georgia Institute of Technology
Atlanta, GA 30332-0245 (USA)
E-mail: zhong.wang@mse.gatech.edu
Dr. B. Hu, Prof. W. Chen
State Key Laboratory of Advanced Technology for Materials Synthesis and Processing
School of Materials Science and Engineering
Wuhan University of Technology
Wuhan, 430070 (P. R. China)
E-mail: chenw@whut.edu.cn

DOI: 10.1002/adma.201002868

© 2010 WILEY-VCH Verlag GmbH & Co. KGaA, Weinheim

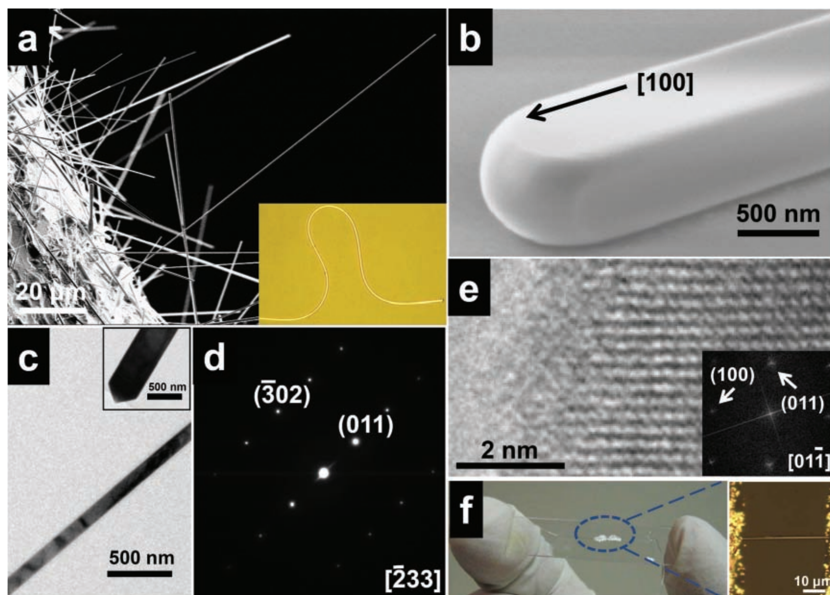

Figure 1. Structural characterization of VO_2 nanobeams and strain sensor fabrication. a) Scanning electron microscopy image of a VO_2 beam grown vertically on the substructure (insert: optical image of the ultra-flexible nanobeams) and b) the detailed morphology shows the smooth surface and rectangular cross sections of the nanobeam. c) TEM image of a VO_2 nanobeam with the inset shows the triangular tip, and d) corresponding selected area electron diffraction pattern in (c) indexed using a [$\bar{2}$ 33] zone axis. e) High-resolution TEM image of a VO_2 nanobeam tip (inset: the corresponding fast Fourier transform pattern indexed to VO_2 with a [01 $\bar{1}$] zone axis). f) As-fabricated strain sensor device and the enlarged optical image of the bonded nanobeam on the right.

well-defined facets, and the thickness and width are around 500 nm. Transmission electron microscopy (TEM) was applied to characterize the single-crystal structure of a VO_2 nanobeam, which preferentially grew along the [100] direction with the bounding (011) and (01$\bar{1}$) side facets in the M_1 phase, and a triangular tip can be observed (Figure 1c–e). The nanobeam was then bonded to the polystyrene (PS) substrate by silver paste and fabricated into a device shown in Figure 1f.[28,29]

For recording the change in phase with the applied strain, the Raman spectrum was measured at different points along the length of the nanobeam. Five featured positions were chosen to investigate the phase transition before and after loading strain by bending the substrate, and distinct structural phases in the VO_2 nanobeam with their evolution were identified by the peak positions and intensities in the Raman spectra as shown in **Figure 2a**. According to previous reports, the featured peaks of the M_1 phase are located at 388 and 608 cm^{-1}, while peaks of M_2 are located at 432 and 645 cm^{-1} (shown by the dashed line).[30,31] As we know, in the atomic structure of the M_1 phase as shown in Figure 2b, all of the V atoms in the two equivalent sublattices, A and B, are dimerized and tilted from the positions of the R phase. In contrast, the M_2 structure has two types of V chains which are quite different from the M_1 phase, one sublattice is strongly paired along the c_R axis without tilting (c_R is the growth direction of the nanobeam), while another sublattice is tilted and forms zigzag chains along the same direction, but not paired.[11,13] Meanwhile, breaking the crystal lattice symmetry results in a change of the lattice constant. Specifically, on comparison with M_1, a significant change of lattice constant occurs along the c_R axis for the M_2 phase (longer by ~0.3%),[32–34] therefore, the beam has relative large change in length during the phase transition considering the c R axis growth direction of the VO_2 nanobeam.

Previous work demonstrated the stabilization of the M_2 phase by doping or by applying uniaxial compressive strain in the $R_{[110]}$ direction in pure VO_2, which produces a tensile strain along c_R.[11] Many recent works were focused on the evolution of nanometer and micrometer-scale M_1–M_2–R phases and domains on a single facet-bonded VO_2 nanobeam. The competition among three spatial phases, as induced by the surface strain when heating above the MIT temperature, occurs during the transition from insulating phase to metallic phase. The intermediate M_2 phase is a more energetically favorable configuration than the M_1 phase because of its large lattice constant along the longitudinal axis which can release more surface tensile strain that comes from the axis shrinkage of the nanobeam after transition into the R phase.[13,23,24,35] Similarly, we loaded the external mechanical strain in our devices by bending the PS substrate to simulate the above temperature-controlled axial strain. Undoped free-standing VO_2 always has the M_1 phase at room temperature. The presence of the M_2 phase near the fixed ends of the nanobeam before loading strain (as show in position 2 and 5 in Figure 2a) is a result of the presence of localized tensile strain in the nanobeam arising from the electrostatic interaction between the nanobeam and the plastic substrate introduced unintentionally during the fabrication and alignment of the nanobeam. Furthermore, loading the tensile strain by bending the substrate enhanced the intensity of the M_2 peaks while weakening the M_1 peaks (position 1, 2, and 4) and even obliterated them (position 5), which indicates an increase in the fraction of M_2 phase when subjected to higher axial tensile strain.

Different vanadium chain structures in the M_1 and M_2 phases results in a change in the activation energy of the VO_2.[23,36–39] For quantitative analysis of the change, in-situ measurement of the I–V characteristics were carried out in the above single-nanobeam device subjected to different strains. Considering the stability and contamination issue, a thin layer of polydimethylsiloxane (PDMS) was used to package the device before the electrical measurement. The flexible PDMS layer was much thinner compared to the substrate thickness. The device was baked in an oven for 1 h at 40 °C to fully polymerize the PDMS. Use of a low temperature in this step ensured that no additional phase transition occurred in the VO_2 beam, therefore, eliminating residual strain after cooling to room temperature.

One end of the well-packaged devices was affixed tightly on a sample holder standing on an optical table and the other end was free for strain loading. A three-dimensional mechanical manipulation stage with a displacement resolution of 1 µm was used to bend the device for loading strain. Equation (1)

© 2010 WILEY-VCH Verlag GmbH & Co. KGaA, Weinheim

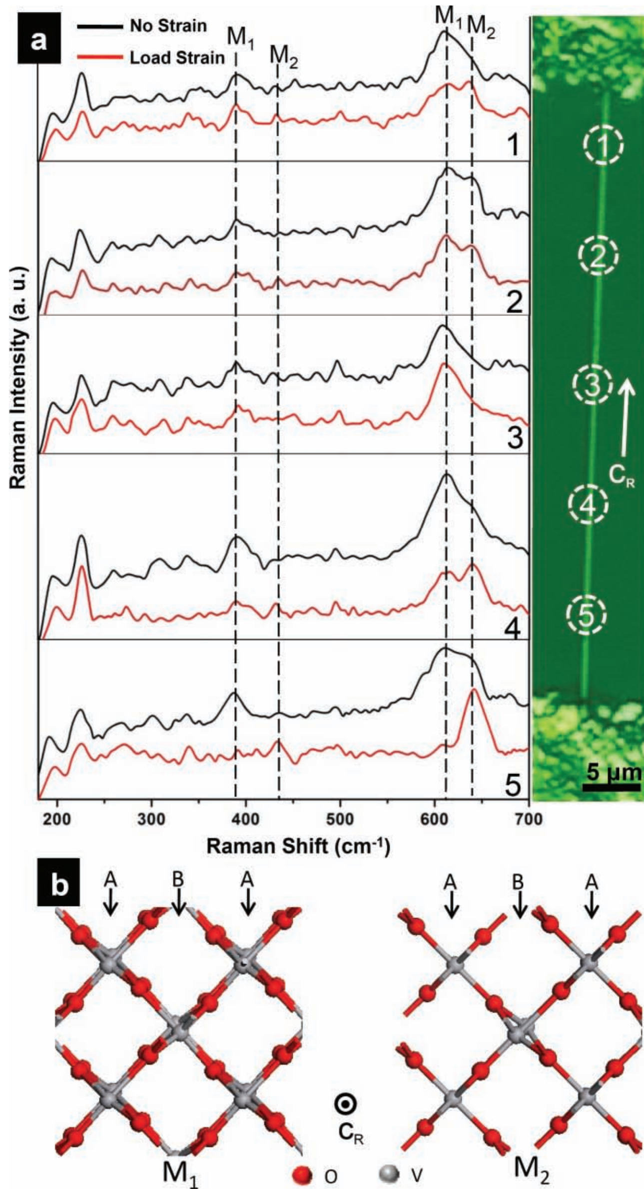

Figure 2. a) Raman spectra acquired from five points along a single VO_2 nanobeam before (upper black line) and after (lower red line) loading tensile strain, which shows the insulating phase transition with the strain. The straight dashed lines distinguish different Raman peaks belonging to the M_1 and M_2 phases; the dashed circles marked in the optical image on the right-hand side show the corresponding recording positions of the Raman spectra along the nanobeam. b) Schematic of the projected atomic structures of VO_2 along the *c*-axis of the rutile phase (c_R) showing the different V chains in the M_1 and M_2 phases.

describes the linear relationship between maximum deflection and the strain loaded on nanobeams:[40]

$$\varepsilon_{zz} = 3\frac{a}{l}\frac{D_{\max}}{l}\left(1-\frac{z}{l}\right) \tag{1}$$

where z and l are the vertical distance from the fixed end of the substrate to the middle of the nanobeams and the free end of the substrate, respectively; a is the half-thickness of the PS substrate; and $D_{\max}$ is the maximum deformation of the free end of the PS substrate. Here, we define the compressive and tensile strain as the negative and positive sign, respectively. With consideration of the much smaller size (length and thickness) of nanobeams in comparison to that of the PS substrate, it is safe to regard the deformation of nanobeams as pure stretching or compressing when the PS substrate was bent.

The original *I–V* characteristic of the device was studied before the electromechanical measurements, and a low voltage (1 V) was applied to eliminate the phase transition induced by Joule self-heating of the nanobeam.[4,41] Similar to using complex photolithography and sputtered Ti/Au to obtain an Ohmic contact,[5,35] most of the 70 or more devices fabricated using silver paste as the electrodes exhibited linear *I–V* characteristics as shown in **Figure 3a**, which indicates that no barriers formed

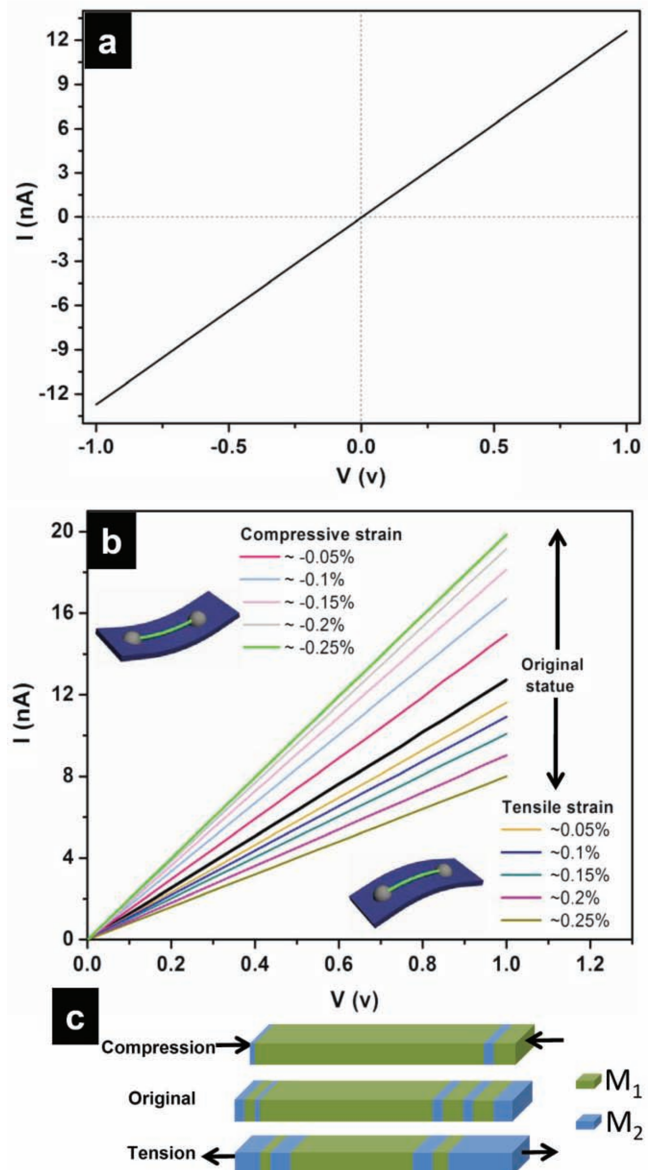

Figure 3. a) The original *I–V* characteristic of the device and b) the *I–V* curve under different tensile and compressive strains. c) Schematic of the phase transition of M_1 and M_2 with tensile and compressive strain.

between the nanobeams and silver electrodes. After consideration of the several factors involved in the *I–V* characteristics of the device, such as contact state, Schottky barrier height, contact area, and crystal growth orientation,[42] the Ohmic contact in the VO_2 devices were found to be relatively stable and reproducible, thereby making it ideal for a three-dimensional strain sensor like an optical fiber strain gauge.

Owing to the symmetric behavior of the *I–V* curve measured in an as-prepared device, the position voltage region was chosen to study the relationship between the strain and the electrical variation. The device was bent to load the tensile or compressive strain step by step with very little increment (~0.05%) in every step, and it was observed that the change of the *I–V* behavior was solely dependent on the loading strain as shown in Figure 3b. In contrast to the tendency of the piezotronic-based strain sensor,[40] the *I–V* curves of the VO_2 nanobeam shifted downward with tension and upward with compression, these distinct responses to the different types of strain arises from the M_1–M_2 phase transition in the nanobeam as discussed above.

As shown in Figure 3c, with the uniaxial tensile strain along the c_R direction as described in the Raman spectra, the fraction of the M_2 phase increased in order to release the strain in the nanobeam, The corresponding decrease of the conductivity can be understood by the relatively high electrical resistance of the M_2 phase compared to the M_1 phase.[43] In contrast, compressive strain can release the preloaded strain in the nanobeam, which decreases the fraction of the M_2 phase and thus increases the conductivity. In this step, we believe that no rutile phase was formed under the low external-strain condition according to a previous report.[4] Thus, the electrical resistance of the device can be easily tuned by simply controlling the loaded strain to adjust the fraction of M_1 and M_2 phases in the nanobeam.

Figure 4a established a quantitative relationship between loaded strain and the resistance: the resistance increased with tension, while it decreased with compression. Scans repeated three times (original state → tension → release → compressive → release) show the repeatable and stable performance of the nanobeam when subjected to cyclic stretching and compressing. Notably, a pronounced hysteresis was observed when releasing the strain. Specifically, under the same tensile strain, the resistance during the loading process was lower than that in the releasing process, while the trend was the opposite in the compression state. However, more study is needed to identify if this phenomenon arises from the phase transition hysteresis between M_1 and M_2 or the surface defect induced carrier charge effect.

In Figure 4b, the typical change in resistance with the variation of strain for the device is plotted to further confirm the working principle of the device. In the compressive state, the change in the resistance is becoming smaller with the increase of compressive strain, probably because of the reduction of the preloaded tension strain induced M_2 phase, step by step, in a localized region of the nanobeam. In contrast, there was enough original M_1 phase transformed into M_2 with the increase in tensile strain, showing the relatively stable tendency in resistance change. The effect of the contact resistance of VO_2 and silver paste in the experiment can be neglected by in-situ deposition of an Au/Ti layer onto the junctions, which is carefully studied in the Supporting Information. Moreover, this typical result was achieved for over 70 devices, also ruling out the dominant contribution made by the contact resistance.[44]

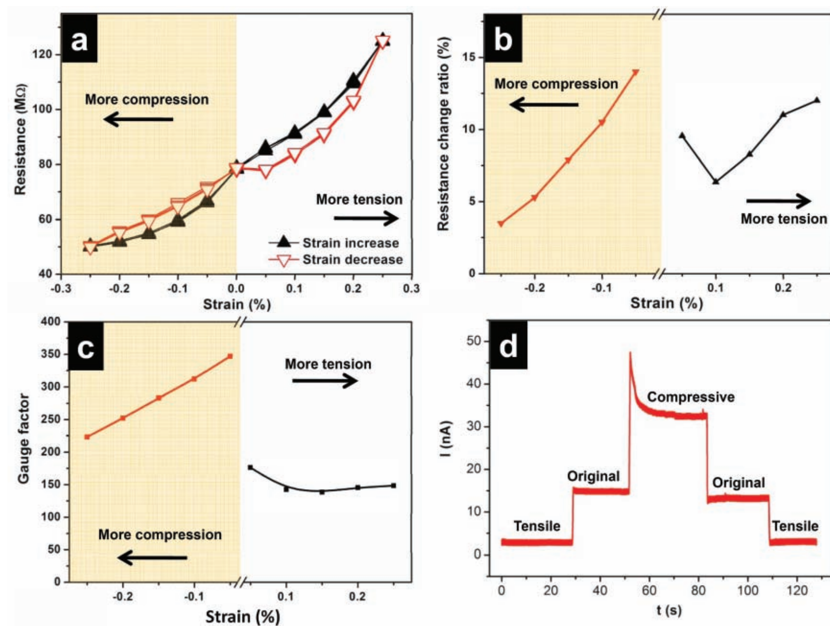

Figure 4. a) The resistance of the nanobeam with different external strain and the release of strain exhibit the hysteresis. b) The change of resistance with the strain from (a) (the resistance variation is defined as absolute value of $\Delta = (R_i - R_{i-1})/R_{i-1}$, where R_i is the resistance measured under current strain status, and R_{i-1} is the resistance under strain in the previous step). c) Gauge factors derived from (a) as a function of strain. d) Quick response to the strain switch.

In addition to the resistance change caused by the phase transition, as discussed above, piezoresistance is another important effect. Under strain, a semiconductor material suffers a small change in band structure, which usually leads to a linear change in resistance based on the first order approximation. This is the mechanism for most semiconductor-based strain sensors. The piezoresistance effect usually has two characteristics. One, it does not introduce the hysteresis effect as observed in Figure 4a, and secondly, the change in resistance is typically a linear relationship with the applied strain, which does not fully agree with the observation shown in Figure 4b. Therefore, we believe that the dominant contribution to the resistance change in our samples is likely a result of a phase transition, although piezoresistance is also possible.

As a type of strain sensor, the performance of the device is characterized by a gauge factor, which is defined to be the slope of the normalized current (I)–strain (ε) curve, $[\Delta I(\varepsilon)/I(0)]/\Delta\varepsilon$. The highest gauge factor for the VO_2 sensor device is 347 (Figure 4c). Interestingly, unlike the gauge

© 2010 WILEY-VCH Verlag GmbH & Co. KGaA, Weinheim

factor for any other type of sensor, the highest gauge factor demonstrated in our sensor device is in the lowest strain. Although it decreases with an increase in strain, it remains higher than the gauge factor of conventional metal strain gauges (1–5) and a doped-Si strain sensor (~200).[40] In addition, the response time was studied under the fixed bias of 1 V as shown in Figure 4d, which a exhibited quick response to the strain switches. Time dependent decay with a sudden loading of compressive strain was probably because of the charge carrier trapping effect. One thing worth noting is that the effect of Joule self-heating of the nanobeam in the above measurement can be excluded, because the current had no shift under the 1 V fixed bias voltage in the all original, compressive, and tensile states. Combining the relative balanced performance in both tensile and compressive states, our device is suitable to serve as a sensor in a low mechanical strain range.

In summary, a free-standing VO_2 nanobeam has been applied to fabricate a flexible strain sensor by utilizing the phase transition between M_1 and M_2 phases. Raman spectra provided evidence for the presence of a localized M_2 phase in the nanobeam, which was induced by the preloaded tensile strain while manipulating its alignment over the substrate. By further loading the external strain, the M_2 phase fraction can be tuned and the resistance of the nanobeam can be controlled. The high gauge factor in low strain ranges with short response time shows the potential application of the VO_2 nanobeam for quantifying small strain. Based on many previous reports involving heating of VO_2 for the desired phase transition,[3,5,13,24,35,45,46] our study demonstrated a transition at room temperature, which can help to understand the electrical properties and the insulating phase transition in VO_2 nanobeams.

Experimental Section

Materials Preparation and Phase Characterization: Single-crystal vanadium oxide nanobeams were grown by modified physical vapor deposition as described previously.[26] VO_2 (0.2 g, 99.9%, Aldrich) powder was placed at the center of a horizontal vacuum tube furnace as the source. After evacuation to a pressure of about 8 torr, the temperature in the center of the tube was elevated to 900 °C, and then high-purity Ar carrier gas (99.999%) was flowed through the furnace at 30 sccm. A Si substrate coated with SiO_2 (500 nm thickness) was placed downstream in a lower temperature region in the furnace approximately 3 cm away from the source, and was tilted into a specific angle with the flow direction of gas. After 2 h holding at 900 °C for nanobeam growth, the samples were allowed to cool to room temperature in flowing Ar. A WITec (Alpha 300R) confocal Raman microscope using an Ar+ ion laser ($\lambda = 514.5$ nm) as an excitation source was used to investigate the phase transition before and after loading strain. The spectrum was obtained using a 600 grooves mm^{-1} grating with a resolution of 3 cm^{-1}. Focusing of the objective was done with a 50x objective (Olympus 50X-NA = 0.75). Spectra were collected with incident beam polarization oriented parallel to the length of the nanobeam.

Device Fabrication: A long and robust VO_2 nanobeam was chosen to fabricate the device for loading strain on the nanobeam. The nanobeam was mechanically transferred from the silicon wafer to a flexible PS substrate with a thickness of ~0.5 mm, length of ~4 cm, and width of ~2 cm. The lengths of the nanobeams were over 50 μm. Moreover, to load strain properly along the axis of the nanobeam, it was placed parallel to the length of the substrate as manipulated by a probe. Silver paste tightly bonded the nanobeams at the two ends onto the substrate which was then baked at 30 °C for 2 h to improve the contact. The silver paste was also used as source and drain electrodes in electrical measurement.

Supporting Information

Supporting Information is available from the Wiley Online Library or from the author.

Acknowledgements

This work was supported by DARPA, DOE BES, and the National Nature Science Foundation of China (No: 50172152). B.H. thanks the China Scholarship Council for support. The authors acknowledge Prof. L. Q. Mai, R. S. Yang, J. H. Song, C. Xu, and F. R. Fan for helpful discussions.

Received: August 7, 2010
Published online:

[1] M. M. Qazilbash, M. Brehm, G. O. Andreev, A. Frenzel, P. C. Ho, B.-G. Chae, B.-J. Kim, S. J. Yun, H.-T. Kim, A. V. Balatsky, O. G. Shpyrko, M. B. Maple, F. Keilmann, D. N. Basov, *Phys. Rev. B* **2009**, *79*, 075 107.
[2] A. Tselev, E. Strelcov, I. A. Luk'yanchuk, J. D. Budai, J. Z. Tischler, I. N. Ivanov, K. Jones, R. Proksch, S. V. Kalinin, A. Kolmakov, *Nano Lett.* **2010**, *10*, 2003.
[3] J. Wei, Z. H. Wang, W. Chen, D. H. Cobden, *Nat. Nanotechnol.* **2009**, *4*, 420.
[4] J. Cao, E. Ertekin, V. Srinivasan, W. Fan, S. Huang, H. Zheng, J. W. L. Yim, D. R. Khanal, D. F. Ogletree, J. C. Grossmanan, J. Wu, *Nat. Nanotechnol.* **2009**, *4*, 732.
[5] J. Q. Wu, Q. Gu, B. S. Guiton, N. P. de Leon, O. Y. Lian, H. Park, *Nano Lett.* **2006**, *6*, 2313.
[6] F. J. Morin, *Phys. Rev. Lett.* **1959**, *3*, 34.
[7] M. M. Qazilbash, M. Brehm, B. G. Chae, P. C. Ho, G. O. Andreev, B. J. Kim, S. J. Yun, A. V. Balatsky, M. B. Maple, F. Keilmann, H. T. Kim, D. N. Basov, *Science* **2007**, *318*, 1750.
[8] J. M. Baik, M. H. Kim, C. Larson, C. T. Yavuz, G. D. Stucky, A. M. Wodtke, M. Moskovits, *Nano Lett.* **2009**, *9*, 3980.
[9] E. Strelcov, Y. Lilach, A. Kolmakov, *Nano Lett.* **2009**, *9*, 2322.
[10] H. T. Kim, B. J. Kim, S. Choi, B. G. Chae, Y. W. Lee, T. Driscoll, M. M. Qazilbash, D. N. Basov, *J. Appl. Phys.* **2010**, *107*, 023 702.
[11] J. P. Pouget, H. Launois, J. P. Dhaenens, P. Merenda, T. M. Rice, *Phys. Rev. Lett.* **1975**, *35*, 873.
[12] K. W. Lee, H. Kweon, J. Park, C. E. Lee, *Appl. Phys. Lett.* **2009**, *94*, 233 111.
[13] J. I. Sohn, H. J. Joo, D. Ahn, H. H. Lee, A. E. Porter, K. Kim, D. J. Kang, M. E. Welland, *Nano Lett.* **2009**, *9*, 3392.
[14] E. U. Donev, J. I. Ziegler, R. F. Haglund, L. C. Feldman, *J. Opt. A-Pure Appl. Opt.* **2009**, *11*, 125 002.
[15] S. Singamaneni, M. Gupta, R. Yang, M. M. Tomczak, R. R. Naik, Z. L. Wang, V. V. Tsukruk, *ACS Nano* **2009**, *3*, 2593.
[16] A. M. Rao, E. Richter, S. Bandow, B. Chase, P. C. Eklund, K. A. Williams, S. Fang, K. R. Subbaswamy, M. Menon, A. Thess, R. E. Smalley, G. Dresselhaus, M. S. Dresselhaus, *Science* **1997**, *275*, 187.
[17] S. M. Bachilo, M. S. Strano, C. Kittrell, R. H. Hauge, R. E. Smalley, R. B. Weisman, *Science* **2002**, *298*, 2361.
[18] M. Z. Atashbar, S. Singamaneni, *Appl. Phys. Lett.* **2005**, *86*, 123 112.
[19] P. J. Pauzauskie, D. Talaga, K. Seo, P. Yang, F. Lagugné-Labarthet, *J. Am. Chem. Soc.* **2005**, *127*, 17 146.

© 2010 WILEY-VCH Verlag GmbH & Co. KGaA, Weinheim

[20] T. Livneh, J. Zhang, G. Cheng, M. Moskovits, *Phys. Rev. B* **2006**, *74*, 035 320.
[21] Z. L. Wang, *J. Nanosci. Nanotechnol.* **2008**, *8*, 27.
[22] U. Ozgur, Y. I. Alivov, C. Liu, A. Teke, M. A. Reshchikov, S. Dogan, V. Avrutin, S.-J. Cho, H. Morkoc, *J. Appl. Phys.* **2005**, *98*, 041301.
[23] S. Zhang, J. Y. Chou, L. J. Lauhon, *Nano Lett.* **2009**, *9*, 4527.
[24] A. C. Jones, S. Berweger, J. Wei, D. Cobden, M. B. Raschke, *Nano Lett.* **2010**, *10*, 1574.
[25] M. Rini, A. Cavalleri, R. W. Schoenlein, R. López, L. C. Feldman, J. R. F. Haglund, L. A. Boatner, T. E. Haynes, *Opt. Lett.* **2005**, *30*, 558.
[26] B. S. Guiton, Q. Gu, A. L. Prieto, M. S. Gudiksen, H. Park, *J. Am. Chem. Soc.* **2005**, *127*, 498.
[27] W. Fan, S. Huang, J. Cao, E. Ertekin, C. Barrett, D. R. Khanal, J. C. Grossman, J. Wu, *Phys. Rev. B* **2009**, *80*, 241 105.
[28] R. S. Yang, Y. Qin, L. M. Dai, Z. L. Wang, *Nat. Nanotechnol.* **2009**, *4*, 34.
[29] J. Zhou, P. Fei, Y. D. Gu, W. J. Mai, Y. F. Gao, R. Yang, G. Bao, Z. L. Wang, *Nano Lett.* **2008**, *8*, 3973.
[30] P. Schilbe, *Phys. B: Conden. Matter* **2002**, *316–317*, 600.
[31] C. Marini, E. Arcangeletti, D. Di Castro, L. Baldassare, A. Perucchi, S. Lupi, L. Malavasi, L. Boeri, E. Pomjakushina, K. Conder, P. Postorino, *Phys. Rev. B* **2008**, *77*, 235 111.
[32] M. Marezio, D. B. McWhan, J. P. Remeika, P. D. Dernier, *Phys. Rev. B* **1972**, *5*, 2541.
[33] D. B. McWhan, M. Marezio, J. P. Remeika, P. D. Dernier, *Phys. Rev. B* **1974**, *10*, 490.
[34] D. Kucharczyk, T. Niklewski, *J. Appl. Crystallogr.* **1979**, *12*, 370.
[35] J. Cao, W. Fan, H. Zheng, J. Wu, *Nano Lett.* **2009**, *9*, 4001.
[36] H. W. Verleur, A. S. Barker, C. N. Berglund, *Phys. Rev.* **1968**, *172*, 788.
[37] W. H. Rosevear, W. Paul, *Phys. Rev. B* **1973**, *7*, 2109.
[38] A. V. Puchkov, M. C. Schabel, D. N. Basov, T. Startseva, G. Cao, T. Timusk, Z. X. Shen, *Phys. Rev. Lett.* **1998**, *81*, 2747.
[39] G. A. Thomas, D. H. Rapkine, S. A. Carter, A. J. Millis, T. F. Rosenbaum, P. Metcalf, J. M. Honig, *Phys. Rev. Lett.* **1994**, *73*, 1529.
[40] J. Zhou, Y. D. Gu, P. Fei, W. J. Mai, Y. F. Gao, R. S. Yang, G. Bao, Z. L. Wang, *Nano Lett.* **2008**, *8*, 3035.
[41] H. T. Kim, B. G. Chae, D. H. Youn, G. Kim, K. Y. Kang, S. J. Lee, K. Kim, Y. S. Lim, *Appl. Phys. Lett.* **2005**, *86*, 242 101.
[42] Z. Y. Zhang, K. Yao, Y. Liu, C. H. Jin, X. L. Liang, Q. Chen, L. M. Peng, *Adv. Funct. Mater.* **2007**, *17*, 2478.
[43] J. Cao, Y. Gu, W. Fan, L. Q. Chen, D. F. Ogletree, K. Chen, N. Tamura, M. Kunz, C. Barrett, J. Seidel, J. Wu, *Nano Lett.* **2010**, *10*, 2667.
[44] P. Fei, P. H. Yeh, J. Zhou, S. Xu, Y. F. Gao, J. H. Song, Y. D. Gu, Y. Y. Huang, Z. L. Wang, *Nano Lett.* **2009**, *9*, 3435.
[45] C. J. Patridge, T.-L. Wu, C. Jaye, B. Ravel, E. S. Takeuchi, D. A. Fischer, G. Sambandamurthy, S. Banerjee, *Nano Lett.* **2010**, *10*, 2448.
[46] J. I. Sohn, H. J. Joo, A. E. Porter, C. J. Choi, K. Kim, D. J. Kang, M. E. Welland, *Nano Lett.* **2007**, *7*, 1570.

© 2010 WILEY-VCH Verlag GmbH & Co. KGaA, Weinheim